"On-the-Fly" Radiometric Calibration of Active 3D Imaging Setups using Superellipse Fitting

James Taylor,[1,*] Jiazhang Wang,[2] Florian Willomitzer[1]

[1] *Wyant College of Optical Sciences, University of Arizona, Tucson, Arizona, USA*
[2] *Department of Electrical and Computer Engineering, Northwestern University, Evanston, Illinois, USA*

[*] *jrt4@arizona.edu*

Abstract: We present a novel approach for the radiometric calibration of phase-measuring 3D sensors. Our approach can be applied to a broad variety of scenes and calculates the calibration parameters "on-the-fly" from the actual object measurement images, meaning that no additional calibration session is required.

1. Introduction

Fringe pattern analysis is a popular and widely used method in many active 3D imaging principles, including phase measuring triangulation (structured light), deflectometry, or interferometry. Although the fundamental physical working principle of these methods is vastly different [1], they all use fringe pattern analysis to calculate the phase of a sinusoidal intensity pattern. Commonly, the phase is calculated from a series of camera images, taken while the sinusoidal pattern is shifted in phase. A popular method is, e.g., the "4-phaseshift algorithm" [2]. A well-known source of error in many phase-measuring 3D imaging systems (e.g., phase measuring triangulation (PMT), or phase-measuring deflectometry (PMD)) is the lack of a proper radiometric calibration of camera and illumination. The "sensitivity gamma curves" of cameras and the "emission gamma curves" of illumination sources (such as displays or projectors) are commonly "non-linear". If not corrected, this "nonlinear gamma parameter" leads to the fact that projected/displayed sinusoidal intensity profiles will not look sinusoidal anymore in the camera image, since they are distorted in their intensity distribution. As the fringe analysis algorithm expects perfect sinusoidal profiles, this error leads to "ripple-artifacts" in the 3D data (see Fig.1.(a)).

A variety of radiometric calibration techniques have proven effective in correcting this nonlinear intensity transformation. These techniques are often broadly categorized into active or passive radiometric calibration methods. Active radiometric calibration usually involves the pre-adjustment of pixel intensity of the projected patterns based on a previously calculated nonlinear gamma curve [3], or bypassing the adjustment problem with defocused dithering projection [4]. Passive radiometric calibration refers to methods that correct after the measurement image is taken, using previously calculated projector-camera response functions [5] or phase look-up tables [6]. All methods that use previous calculation of the gamma curve require a large set of images that needs to be taken during a separate calibration routine *before* the actual 3D measurement. This procedure must be repeated in some cases if the scene changes, e.g., if objects with a different reflectance have to be measured. All this makes radiometric calibration a relatively cumbersome process that is still prone to error for scenes with varying reflectance.

In this paper we introduce a novel radiometric calibration procedure that can be performed "on-the-fly". This means that no additional measurements need to be taken during a separate calibration routine - the images taken for the 3D measurements themselves deliver the input information for our calibration method. In turn, this also means that our method is robust against vastly varying reflectance conditions in the scene, as each single 3D measurement calculates its own radiometric calibration parameters in each single pixel separately "on the fly".

2. Method, Results, and Outlook

Our method uses a phase error correction technique inspired by the Lissajous ellipse-to-circle algorithm presented in [7]. This algorithm was originally developed to compensate spatial phase shift errors in polarization-based

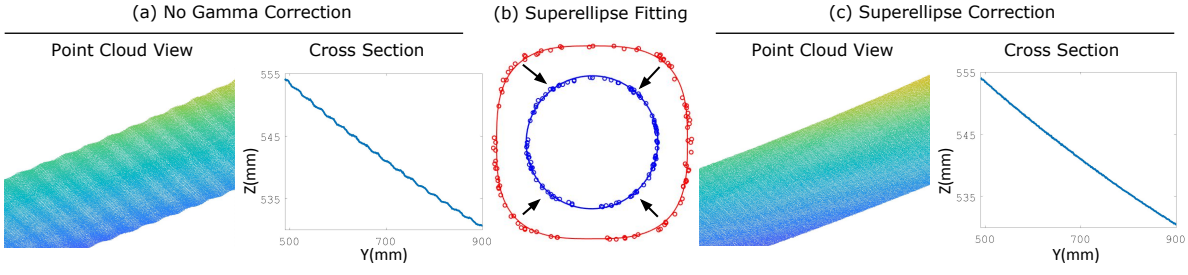

Fig. 1: **Radiometric calibration by superellipse fitting.** (a) Reconstructed surface without radiometric calibration. (b) In red: Example for plotted and fitted superellipse to the raw captured data. In blue: Plot of corrected data after removing the nonlinear distortion. (c) Reconstructed surface after on-the-fly radiometric calibration.

interferometry. Herein, we modify the idea towards an "on-the-fly" gamma calibration of illumination and camera. In the following, we focus our explanations around the 3D imaging method phase-measuring triangulation (PMT), although our principle is universal and can also be applied to other 3D imaging methods that rely on fringe pattern analysis. Moreover, we demonstrate our method at the example of the well-known "4-phaseshift algorithm" [2].

As shown in [8], we model the captured distorted fringes as exponentiated sinusoids. Consequently, the intensity captured in each camera pixel (x,y) for a 4-phase shifted sinusoidal fringe image that is projected onto a surface can be written as:

$$I_n(x,y) \quad = \quad [R(x,y)[C(x,y)+[A+Bsin(\phi(x,y)+\frac{n\pi}{2})]^p)]^c, \qquad n=[0,3]. \tag{1}$$

R is the surface reflectance, C is the background intensity, A is the projector intensity offset, B is the amplitude of the sinusoidal modulation, and p and c denote the projector and camera nonlinear responses, respectively. In this paper, we approximate the background intensity C as zero for the sake of brevity and simplification. In our experiments, $C \approx 0$ can be reached for scenes without or with minimal inter-reflections and measurements in dark rooms. The full mathematical formulation for $C \neq 0$ will be described in a follow-up publication.

As discussed, the 4-phaseshift algorithm delivers a wrong calculated phase $\phi_{wrong}(x,y)$ because of the uncompensated non-linearities in observation and projection. Assuming $C \approx 0$, $\phi_{wrong}(x,y)$ can be expressed as

$$\phi_{wrong}(x,y) = arctan(\frac{I_1-I_3}{I_2-I_4}) = arctan(\frac{G_1(sin(\phi))^g}{G_2(cos(\phi))^g}), \qquad g = p \cdot c \tag{2}$$

where ϕ is the correct (true) phase, and G_1 and G_2 are functions of A, B, and g. Plotting the numerator of this *arctan*-function along the x-axis and the denominator along the y-axis delivers a superellipse for every single surface reflectance value R . The exponent of this superellipse is now directly related to the nonlinear gamma parameters and G_1 and G_2 correspond to the width and the height of each superellipse. In turn, this means that we can estimate g, as well as G_1 and G_2 via superellipse-fitting (see Fig.1.(b)). The basic procedure is as follows: To plot a super ellipse for each surface reflectance value, we find scene points with similar reflectance by calculating the mean intensity $\bar{I} = \sum_{n=0}^{4} I_n/4$ and choosing pixels with similar mean intensity as sample points. After plotting the respective superellipe for our sample points (see, e.g., red superellipse in Fig.1.(b)), we iterate through different gamma parameters and apply the inverse of those parameters to our nominator and denominator in Eq.2. The correct g is found if the superellipse turns into a circle (blue circle in Fig.1.(b)). Applying the inverse gamma parameters, the correct phase value ϕ can now be calculated from Eq.2.

To demonstrate the effectiveness of our method, we measure a slightly curved piece of cardboard with an uncalibrated PMT setup. Evaluating the 3D point cloud with the uncompensated 4-phaseshift-algorithm leads to the discussed prominent ripples in the data (see Fig.1.(a)). From the captured measurment images (no extra calibration images necessary), we fit superellipses (Fig.1.(b)) and perform our on-the-fly radiometric calibration. No remaining ripple-artifacts can be seen in the resulting 3D data (Fig.1.(c)) after correction.

In a future publication, we will further extend the mathematical formulation of our novel calibration method towards more general cases. Moreover will show quantitative evaluations of measurements of complicated scenes with mixed reflectance to further demonstrate the potential of our method.

Acknowledgement: The authors thank Aniket Dashpute for his assistance in preparing this manuscript.

References

1. Gerd Häusler and Florian Willomitzer. Reflections about the holographic and non-holographic acquisition of surface topography: where are the limits? *Light: Advanced Manufacturing*, 3(2):226–235, 2022.
2. Katherine Creath. V phase-measurement interferometry techniques. volume 26 of *Progress in Optics*, pages 349–393. Elsevier, 1988.
3. Xu Zhang, Limin Zhu, Youfu Li, and Dawei Tu. Generic nonsinusoidal fringe model and gamma calibration in phase measuring profilometry. *J. Opt. Soc. Am. A*, 29(6):1047–1058, Jun 2012.
4. Xian-Yu Su, Wen-Sen Zhou, G. von Bally, and D. Vukicevic. Automated phase-measuring profilometry using defocused projection of a ronchi grating. *Optics Communications*, 94(6):561–573, 1992.
5. Paul E. Debevec and Jitendra Malik. Recovering high dynamic range radiance maps from photographs. In *Proceedings of the 24th Annual Conference on Computer Graphics and Interactive Techniques*, SIGGRAPH '97, page 369–378, USA, 1997. ACM Press/Addison-Wesley Publishing Co.
6. Thang Hoang, Bing Pan, Dung Nguyen, and Zhaoyang Wang. Generic gamma correction for accuracy enhancement in fringe-projection profilometry. *Opt. Lett.*, 35(12):1992–1994, Jun 2010.
7. Brad Kimbrough. Correction of errors in polarization based dynamic phase shifting interferometers. *International Journal of Optomechatronics*, 8(4):304–312, 2014.
8. Gaoxu Deng, Shiqian Wu, Lingyun Zou, Wei Cao, and Zhonghua Wan. A gamma self-correction method via chord distribution coding in fringe projection profilometry. *Electronics Letters*, 58(8):315–317, 2022.